08,11,03

The electrical resistance of laser-induced graphene synthesized by a continuous-wave CO_2-laser

© K.G. Mikheev, R.G. Zonov, N.V. Chuchkalov, G.M. Mikheev

Udmurt Federal Research Center, Ural Branch Russian Academy of Sciences,
Izhevsk, Russia

E-mail: k.mikheev@udman.ru

Received January 15, 2024
Revised January 15, 2024
Accepted January 17, 2024

Laser-Induced Graphene (LIG) is a promising new material for widespread applications in electronics and medicine. This study presents experimental results on measuring its specific conductivity (σ), sheet resistance (R_s), as well as contact resistance (R_c) and specific contact resistance (ρ_c) of a copper electrode with the LIG film structure synthesized on the surface of a polyimide film using the method of its near-surface layer pyrolysis through line-by-line scanning of a focused beam of cw carbon dioxide laser. It is established that the synthesized LIG film structure exhibits anisotropy in electrical resistance, attributed to the line-by-line scanning. It is demonstrated that σ, R_s, R_c, and ρ_c significantly depend on the fluence (F) of the incident laser radiation. Measured values of σ, R_s, and ρ_c varied in the ranges of $7.7 \div 10$ S/cm, $26 \div 49\,\Omega$/sq, and $9 \div 43\,\Omega \cdot \text{mm}^2$, respectively, with an increase in F from 31 to 137 J/cm^2.

Keywords: sheet resistance, specific conductivity, contact resistance, specific contact resistance, electrical anisotropy.

DOI: 10.61011/PSS.2024.02.57924.5

1. Introduction

Laser-induced graphene (LIG) is a novel material, representing three-dimensional porous graphene [1–3]. It can be synthesized by pyrolysis of the carbon-containing precursor in an open air atmosphere without creating special conditions using a low-power cw carbon dioxide laser [4–6]. A popular precursor for these purposes is polyimide (PI) film with a chemical structure consisting of aromatic and imide repeating units [7]. The use of other carbon-containing materials for LIG synthesis is known (see, for example, [8–10]). Easy of synthesis and unique physicochemical properties of LIG (high specific surface area — 340 m^2/g, high thermal stability — $> 900^\circ$C, good electrical conductivity — $5 \div 25$ S/cm) [11] makes it attractive for use in various fields of technic, including mechanics [12], electronics [11,13–19], optoelectronics [20,21] and medicine [22,23]. For example, LIG can be employed in the development and creation of various flexible electronic devices for continuous monitoring of human physiological parameters throughout daily activities [14,24,25]. One of such devices is a strain sensor, the operating principle of which is based on measuring the changed during stretching electrical resistance of the LIG film structure transferred onto the elastic base [26,27]. At the same time, LIG has the properties of semiconductor. When measuring its electrical resistance using the two-point method, the result obtained may depend on the contact resistance R_c [28] that occurs between LIG and measuring metal probe, typically made, for example, of copper. In turn, R_c depends on the specific contact resistance ρ_c, which has the dimension $\Omega \cdot \text{mm}^2$ [29]. However, despite the large number of publications on the study of LIG, currently there are no papers aimed at determining ρ_c between LIG and metal electrodes.

The purpose of this paper is to study the electrical characteristics of LIG film structure synthesized using the cw CO_2-laser on the surface of PI film at different fluence of incident radiation. The conducted research demonstrated that the sheet resistance of LIG, as well as the contact resistance and specific contact resistance of LIG with copper electrode noticeably depend on the laser radiation fluence used in LIG synthesis. Using the standard four-probe technique, it was determined that the sheet resistances of the synthesized LIG film structure along and perpendicular to the scanning line of the laser beam differ from each other by $5 \div 30\%$ relative to the average value and depending on the laser fluence.

2. Research objects and methods

In our experiments, a commercial PI film was used as a precursor for LIG synthesis with thickness of 100 μm. To obtain flat samples of LIG film structure, PI film strips were fixed to smooth textolite substrates using double-sided adhesive tape. Subsequently, they were irradiated line by line with a focused beam of cw carbon dioxide laser (see Figure 1, *a*), coupled with an automated two-coordinate table, following the technique described in detail in our recent publications [30,31]. The obtained LIG samples had a rectangular shape with dimensions 10×120 mm (see

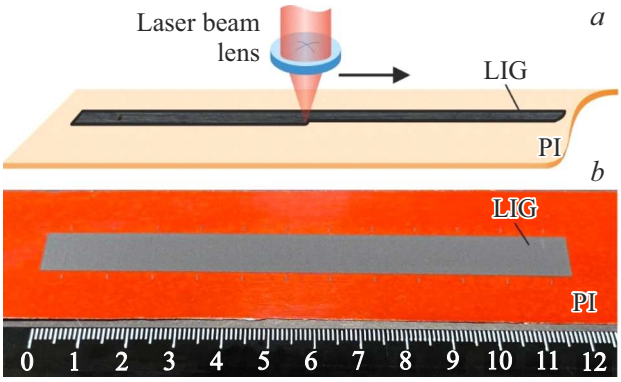

Figure 1. (a) Scheme of LIG synthesis and (b) photograph of the synthesized LIG film structure with dimensions 10×120 mm on the surface of the PI film.

Figure 1, b). During LIG synthesis the focused laser beam with diameter $d = 120\,\mu$m moved parallel to the long side of „drawn" rectangle at a speed of $v = 220$ mm/s. The laser power P incident on the PI film varied in the range $1.7 \div 7.6$ W, and the distance between adjacent lines Δ during line-by-line irradiation was $25\,\mu$m. In this case, the fluence F_1 incident on the PI film during a single line scan and calculated by the equation $F_1 = P/(vd)$ varied within the range $6.4 \div 28.8$ J/cm^2. Taking into account the fact that at beam diameter of d the distance between the lines was Δ, in general the film was formed at the fluence determined by the equation $F = F_1 \cdot (d/\Delta)$ [6]. In this case, F varied within $31 \div 137$ J/cm^2.

The laser power incident on the surface of PI film was measured using a power meter PM100D coupled with a thermal power sensor S425C-L(Thorlabs), sensitive in a wide range of wavelengths $0.19 \div 20\,\mu$m of incident radiation. The surface morphology of the synthesized films was investigated using a Thermo Fisher Scientific Quattro S scanning electron microscope (SEM). To identify the synthesized carbon material, HORIBA HR800 Raman-scattering spectrometer was utilized with exciting radiation from a helium-neon laser at wavelength of 632.8 nm. To avoid large heating in the area affected by the laser beam [32], the power density of the exciting laser radiation was less than 1 kW/cm^2. For each LIG sample more than 10 spectra were measured and subsequently averaged. The averaged spectra underwent background luminescence subtraction and decomposition into individual bands. The thickness of the obtained LIG films was determined using SEM and optical microscope Neophot-32 coupled with ToupCam U3ISPM18000KPA (USB3.0) digital camera. Photographs of the prepared samples were taken using Canon EOS 20D digital camera.

The contact resistance R_c of the synthesized LIG samples was determined by the two-electrode technique proposed by Schottky, which was called „Transmission Line Model Measurements" [33]. The essence of this technique is to extrapolate the experimental dependence of the electrical resistance R_T between two metal electrodes positioned on the surface of the film under study, as a function of the distance between them L, and finding the value R_T at $L = 0$ (see Figure 2, a). In accordance with [33]:

$$R_T = 2R_c + R_s L/Z, \tag{1}$$

where R_s — sheet resistance of the film under study; Z — the width of the electrode, measured along the direction perpendicular to the direction of the flowing current;

$$R_s = \rho/h, \tag{2}$$

ρ and h — resistivity and thickness, respectively, of the film material, R_s has the dimension Ω/sq. From Figure 2 it follows that R_s of the investigated film can be determined from the relation $\mathrm{tg}\,\alpha = R_s/Z$, where α — the slope of the line $R_T(L)$ with respect to the abscissa axis. The value R_T at $L = 0$, found by extrapolating the dependence $R_T(L)$, is $2R_c$. In Figure 2, a one can see that $R_T = 0$ at $L = -2L_T$, where L_T — so called „transfer length" [29]). In accordance with [29] L_T is determined as follows:

$$L_T = (\rho_c/R_s)^{1/2}. \tag{3}$$

Expression for contact resistance is given in [29] as follows

$$R_c = (L_T/Z)R_s \mathrm{coth}(W/L_T), \tag{4}$$

where W — electrode length along current direction (see Figure 2), which is true at $Z \gg W$, $Z \gg L_T$, and if resistance of metal electrodes is neglected. From equation (4) and considering (3), the expression for ρ_c can be obtained in the following form:

$$\rho_c = R_c Z L_T/\mathrm{coth}(W/L_T). \tag{5}$$

For simple calculations, it can be noted that at $W < 0.5L_T$ and $W \geq 1.5L_T$ approximations $\rho_c \approx RcZW$ and $\rho_c \approx R_c Z L_T$ are valid, respectively, as under these conditions $\mathrm{coth}(W/L_T)$ can be well approximated by L_T/W and 1, respectively. In this paper, we used equation (5) for the calculation of ρ_c.

To determine R_c and ρ_c using the aforementioned technique, a special template in the form of an elongated rectangle was made from organic glass (see Figure 2, b). It featured 12 holes, cut using the carbon dioxide laser into narrow rectangles $Z_0 = 10$ mm long and $W_0 = 1$ mm wide. The holes were positioned parallel to each other at a distance of 10 mm along the long side of the template. Thus, the distance between the outermost holes was 110 mm. To measure the dependence of R_T on L, the fabricated template was fixed above the surface of the synthesized film in such a way that a minimal gap remained between the surfaces of the film and the template. Then, the first spring-loaded copper electrode, in the form of the elongated flat rectangular parallelepiped, with dimensions of the measuring part ($Z = 9.2$ mm, $W = 0.68$ mm) close to the linear dimensions of the template holes, was inserted and

fixed into the leftmost hole of the template. Subsequently, a second spring-loaded copper electrode, with linear dimensions matching those of the first electrode, was inserted into the rightmost hole of the template. Both electrodes were pressed against the LIG film under study with a force of 4.3 N creating a pressure of 0.7 N/mm^2 on LIG surface. Note that the electrodes did not leave visible traces on LIG surface. After fixing the electrodes, the electrical resistance of the film between them was measured, i. e. R_T was measured at $L = 110$ mm. Then, the right electrode was moved and installed in an adjacent hole located at a distance of $L = 100$ mm from the left electrode. The resistance R_T between the electrodes was again measured at $L = 100$ mm. This procedure was then repeated eight more times. Thus, it was possible to obtain experimental dependences of R_T on L for LIG film structures synthesized at different laser powers.

At six fixed laser fluence F values, five samples of LIG films were synthesized. Based on the averaged values obtained as a result of processing the experimental data R_T as a function of L, the values R_s, R_c and ρ_c of LIG film structures were determined for each of these values of F.

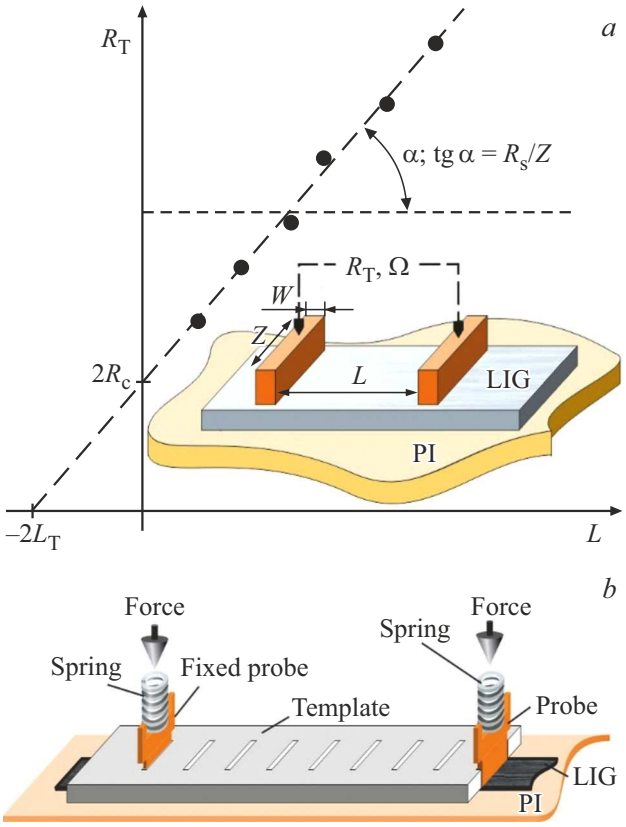

Figure 2. (a) Illustration of the technique for determining the contact resistance R_c and sheet resistance R_s from the measured dependence of resistance R_T between two rectangular electrodes with dimensions $Z \times W$ on the distance L between them, as well as (b) a schematic representation of the LIG film structure and a special template placed on it with holes for fixing spring-loaded measuring electrodes in them.

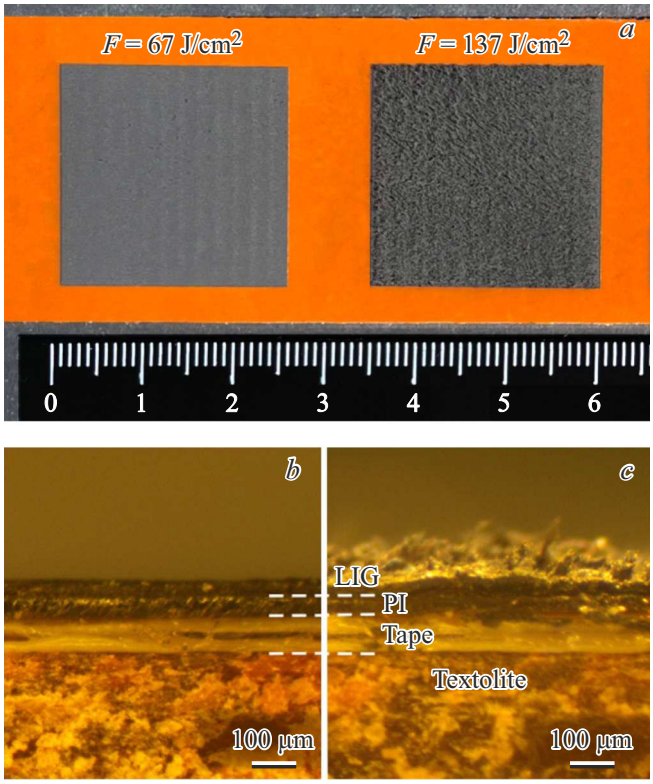

Figure 3. (a) Photographs of two LIG samples of size 25 × 25 mm, synthesized on the surface of PI film at fluences of 67 and 137 J/cm^2 and scanning speed of 220 mm/s, (b) and (c) as well as photographs of their ends, respectively.

The sheet resistance R_s of the synthesized films was additionally measured by the four-probe technique on ST-2258C device using ST2558B-F01 probe having four measuring electrodes located on the same line at a distance of 2 mm from each other (see insert to Figure 7, d). The measuring electrodes of the probe were made in the form of cylindrical tips with base area $S_1 = 1.3$ mm^2, and the pressure under the measuring electrodes was 0.43 N/mm^2. To exclude edge effects, measurements were carried out in the central part of LIG samples of size 25 × 25 mm, photographs of two of which are shown in Figure 3, a.

3. Results and discussion

Figure 3, a shows photographs of LIG samples with size of 25 × 25 mm, synthesized at different fluence F values of laser radiation. They differ from each other in color shade: LIG samples synthesized at high F have a more saturated gray color.

Figure 4, a, b shows SEM images of LIG samples synthesized at $P = 3.7$ W and $P = 7.55$ W, which corresponds to $F = 67$ J/cm^2 and $F = 137$ J/cm^2, respectively. At $F = 67$ J/cm^2 (Figure 4, a) the surface of LIG is almost homogeneous, and represents a porous structure formed due to gases release during pyrolysis. With the fluence

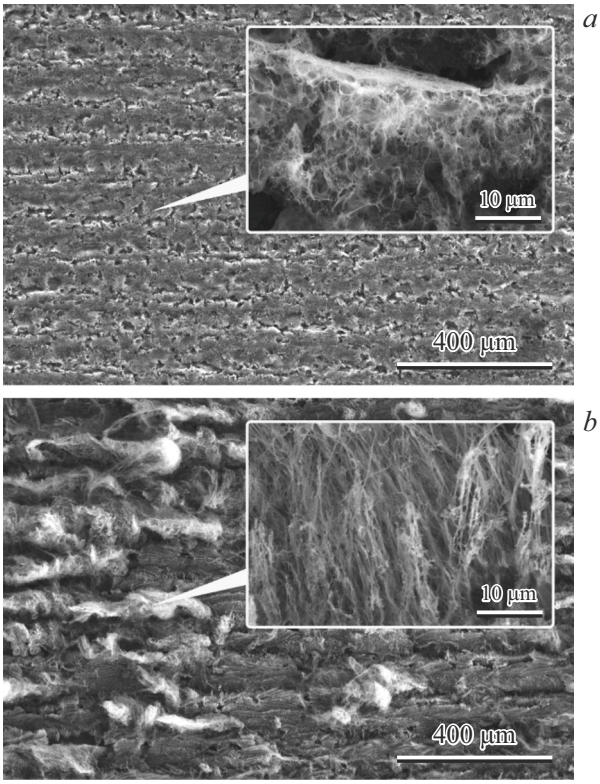

Figure 4. SEM images of surface of LIG synthesized using a *cw* CO_2 laser at fluence of (*a*) 67 and (*b*) 137 J/cm^2. The insets show areas of the corresponding images in an enlarged scale.

increasing, many fibrous formations appear that grow on top of the porous structure (Figure 4, *b*, insert), which was also observed in [34,35]. Due to this, the thickness of LIG increases, which is clearly seen from a comparison of the images of ends of LIG films obtained at $F = 67$ J/cm^2 and $F = 137$ J /cm^2 shown in Figure 3, *b* and Figure 3, *c*, respectively. Thus, with F increasing the structure of LIG changes from porous to fibrous, which leads to increase in LIG thickness.

Figure 5 shows the Raman spectra of LIG film structures synthesized at $F = 31 \div 137$ J/cm^2. For clarity the spectra are normalized to the intensity of the G-band.

It can be seen that all spectra contain bands characteristic of LIG, and described in detail in [30]. The ratios of intensities of D and G bands I_D/I_G, as well as of 2D and G bands I_{2D}/I_G, obtained at different fluences, indicate that the defect density and stacking structure of carbon atoms in LIG vary depending on the laser fluence (see Figure 5, *b*). I_D/I_G reflects the defect density: larger I_D/I_G corresponds to higher LIG defect density [36]. It can be seen that with increase in fluence from 31 to 67 J/cm^2 there is a minor increase in I_D/I_G. With a further increase of F to 110 J/cm^2 there is a sharp decrease in I_D/I_G from 1.9 to 1.2. A subsequent increase in F again leads to increase in I_D/I_G to 1.4. Thus, the minimum number of defects in LIG is observed at $F = 110$ J/cm^2. The ratio I_{2D}/I_G is used to determine the fraction of ordered graphene in LIG [37]: larger I_{2D}/I_G indicates a greater degree of graphenization. In the range of fluence values from 31 to 110 J/cm^2 I_{2D}/I_G remains practically unchanged at the level of 0.6 and decreases sharply at $F = 137$ J/cm^2 to 0.4 (see Figure 5, *b*), which indicates a decrease in the quantity of ordered graphene [37].

The decrease in defect density at $F = 67 \div 110$ J/cm^2 is due to a higher degree of graphitization, i. e. increase in the quantity of ordered sp_2 carbon. Note that in this case no increase in the degree of graphenization is observed. With further increase in F, the porous structure of LIG begins to transform into a fibrous one (see Figures 3, *c* and 4, *b*), which leads to increase in the defect density and decrease in the degree of graphenization.

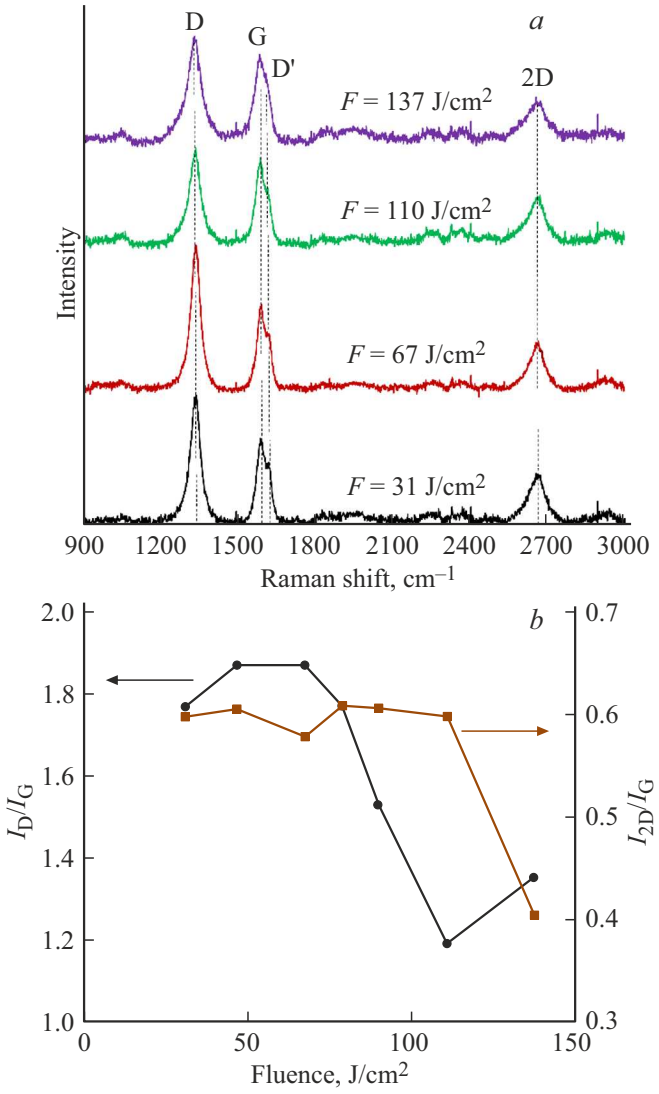

Figure 5. (*a*) Raman spectra of LIG samples synthesized at fluences of 31, 67, 110, 137 J/cm^2, normalized to the intensity of G-band and spaced along the vertical axis for easy perception. (*b*) Dependences of the ratio of intensity D- and G-bandsI_D/I_G (circles) and 2D- and G-bandsI_{2D}/I_G (squares) on fluence.

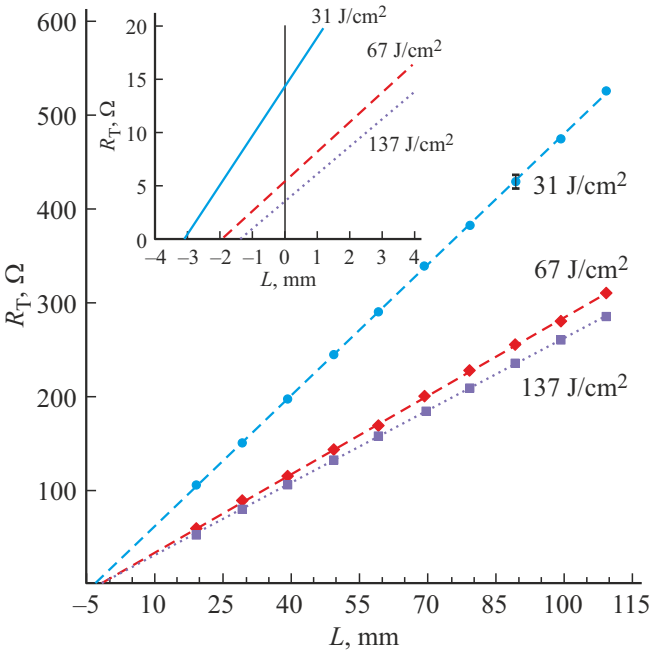

Figure 6. Resistances R_T measured between two copper electrodes on LIG film structure synthesized at different fluences F vs. the distance between them L. The inset shows the corresponding dependences on an enlarged scale near the origin of the two-coordinate system $R_T(L)$.

The measured values of R_T depending on L for LIG samples synthesized at three different values of fluence F are shown in Figure 6. It can be seen that all experimental points $R_T(L)$ obtained for any fixed F are well aligned on a single straight line, withe each line intersecting the ordinate axis at a value greater than zero. This indicates that between the copper electrode and LIG there is contact resistance R_c other than zero. For each selected fluence F approximation of the measured data array $R_T(L, F = \text{const})$ by a rectilinear dependence using the equation (1) allows us to find the values R_s, R_c and L_T, shown schematically in Figure 2, *a*.

The obtained dependencies of R_s and R_c vs. F are shown in Figure 7, *a, b*. Figure 7, *a* shows that with increase in F from 31 to 137 J/cm^2 the noticeable decrease in R_s from 43 to 24 Ω/sq is observed, this is accompanied by more significant decrease in R_c from 7 to 1.8 Ω (see Figure 7, *b*). Note that the dependencies $R_s(F)$ and $R_c(F)$ are nonlinear. Nonlinear decrease in R_s with F increasing is observed in many papers [1,28,38–40], though in some publications [35,41] the experimentally defined dependencies $R_s(F)$ were approximated by linear drop-down functions. Note that R_s, obtained at fixed F, decreases as a result of repeated or multiple scanning by the laser beam over the same LIG surface, which is consistent with the results of the paper [30,42]. A more significant decrease in R_s can be achieved by applying liquid metal to LIG [43].

Taking into account the geometric dimensions of the measuring electrodes (see above), the set of found by equation (5) parameters R_c and L_T allows us to calculate the specific contact resistance ρ_c for each selected value of F. The calculated values ρ_c of LIG depending on F are shown in Figure 7, *c*. It can be seen that the found dependence $\rho_c(F)$ is similar to the dependence $R_c(F)$. At the lowest value of $F = 31$ J/cm^2, at which LIG synthesis is still possible, $\rho_c = 43\ \Omega \cdot \text{mm}^2$, and with F increasing to 137 J/cm^2 specific contact resistance ρ_c decreases by almost five times and amounts to $8.8\ \Omega \cdot \text{mm}^2$. Thus, at a given beam scanning speed, the sheet resistance of the film R_s of the synthesized LIG film structure, as well as the contact resistance R_c and the specific contact resistance ρ_c of LIG/metal decrease with increase in fluence F, at which LIG is formed. Note that in the paper [28] when studying the contact resistance of LIG synthesized using laser diode at the wavelength of 405 nm, no change of R_c was observed with laser power (and therefore fluence) varying. In our experiments, we clearly showed that R_c, and therefore ρ_c, significantly depend on the synthesis conditions, in particular, on the fluence F.

Figure 7, *d* shows the sheet resistance values measured by the four-probe tecnhique for square-shaped LIG samples (see Figure 3), synthesized at various values of F. The measurements were performed with the orientation of a straight line (l) passing through four electrodes of the measuring probe, parallel to ($R_{s,\parallel}$) and perpendicular ($R_{s,\perp}$) to the laser lines (ll). It can be seen that the dependences $R_{s,\perp}(F)$ and $R_{s,\parallel}(F)$ are similar to each other and have decreasing and increasing sections at small and large values F, respectively. However, the sheet resistance $R_{s,\perp}$, obtained at $l \perp ll$, in the entire range F is slightly higher than the sheet resistance $R_{s,\parallel}$, measured at $l \parallel ll$. Thus, LIG synthesized by line-by-line scanning has an anisotropy of sheet electrical resistance. A measure of the anisotropy of sheet resistance can be the parameter $\eta = 2 \cdot (R_{s,\perp} - R_{s,\parallel})/(R_{s,\perp} + R_{s,\parallel})$, its dependence on F is shown in Figure 7, *e*. It can be seen that the parameter η varies from 0.08 to 0.3, and with increase in F the value η increases. Note that the anisotropy of a similar LIG film structure also manifests itself in the angular spectrum of light scattered on its surface [5]. The differences in the electrical characteristics of LIG film structures synthesized during parallel and perpendicular scanning are clearly observed in experiments on their stretching [44], as well as during the generation of photocurrent pulses due to the photon drag effect (PDE) [45]. Figure 7, *f* shows the dependences R_s and $R_{s,\parallel}$ on F, measured by the two-electrode (see above) and the four-probe technhiques at $l \parallel ll$, respectively. It shows that the results of measuring the sheet resistance of samples using the specified methods practically coincide at small values of F, but differ by approximately 50% at $F = 137$ J/cm^2. As can be seen from Figure 7, *f*, such difference arises due to the fact that at $F > 67$ J/cm^{2}dependencies $R_s(F)$ and $R_{s,\parallel}(F)$ decrease and increase respectively. In our opinion, the increasing sections $R_{s,\parallel}(F)$ and $R_{s,\perp}(F)$ (see Figure 7, *d*) can be explained by LIG porosity increasing at large F and the small

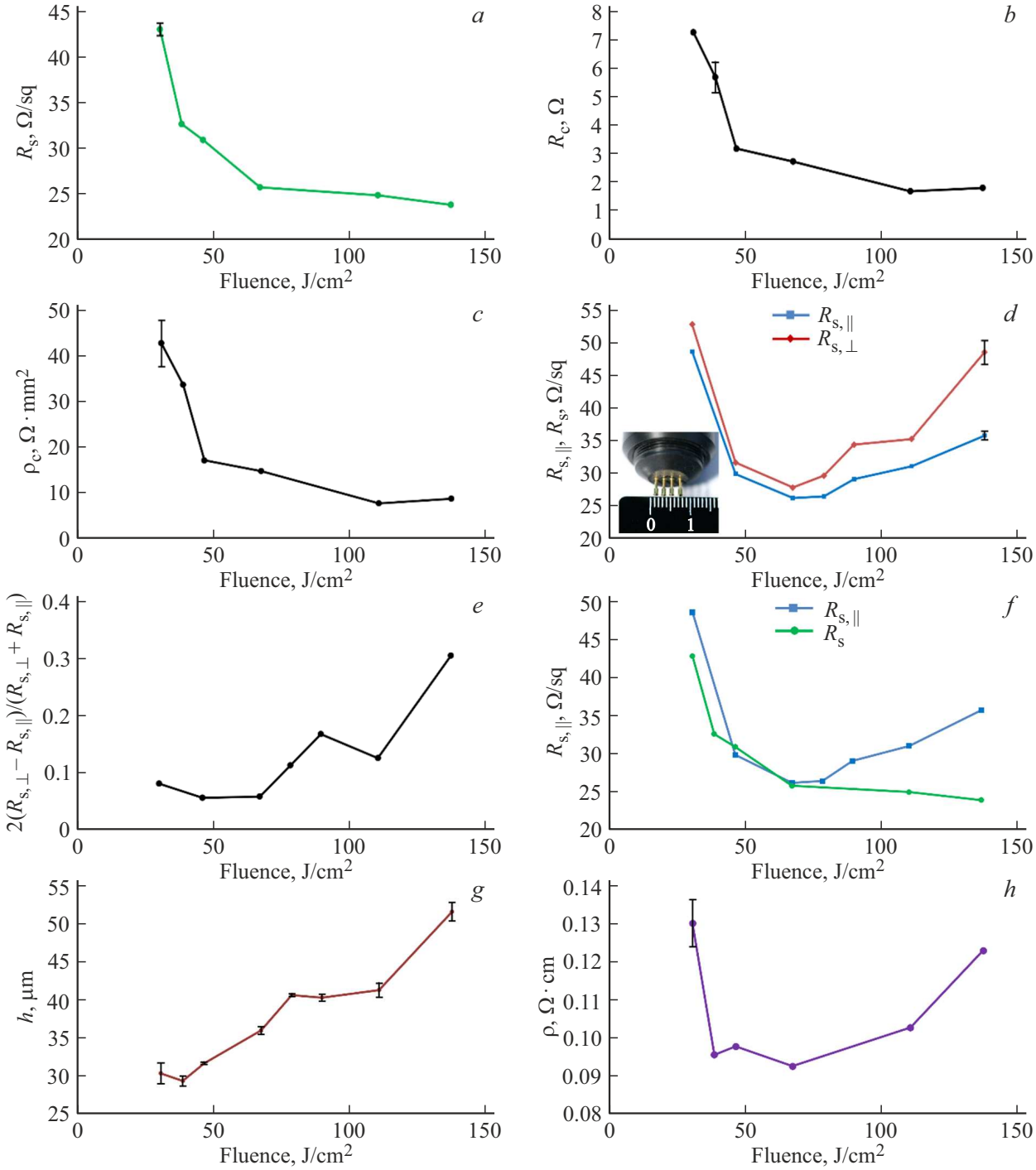

Figure 7. (*a*) Sheet resistance R_s, (*b*) contact resistance R_c and (*c*) specific contact resistance ρ_c of LIG vs. laser fluence F, found from experiments using the two-electrode method. (*d*) Dependences of the sheet resistance $R_{s,\parallel}$ and $R_{s,\perp}$ of LIG film structure, measured by the four-probe technique parallel and perpendicular to the scanning line of the laser beam, respectively, from F; the inset shows photograph of the probe used in the four-probe technique. (*e*) $2(R_{s,\perp}-R_{s,\parallel})/(R_{s,\perp}+R_{s,\parallel})$ vs. F. (*f*) R_s and $R_{s,\parallel}$ vs. F, presented for comparison with each other. (*g*) Thickness h and (*h*) resistivity ρ of LIG vs. F.

cross-section area of the tips of the measuring electrodes ($S_1 = 1.3\,\text{mm}^2$) used when measuring sheet resistance by the four-probe technique. The higher the LIG porosity is, the deeper the measuring electrodes „penetrate“ into it, increasing the area of breaking the electrical contact between LIG and the side surface of the cylindrical tip. In the experiments, the results of which are presented in Figure 6, the cross-section area S_2 of rectangular electrodes in contact with LIG is much larger ($Z = 9.2\,\text{mm}$, $W = 0.68\,\text{mm}$, $S_2 = 6.3\,\text{mm}^2$), and therefore the break of

the electrical contact between LIG and the electrode is lesser.

A decrease in R_s with increase in F, in accordance with equation (2), can be associated with simultaneous changes in electrical resistivity ρ and thickness h of LIG film material. The results of the experiments carried out to measure h are presented in Figure 7, *g*. It shows that with F increasing there is a gradual increase in thickness h, which, in accordance with equation (2), shall lead to decrease in R_s (see Figure 7, *a*). In our experiments, measurements of R_s and h at different values of F were carried out by independent methods. So, from the dependencies $R_s(F)$ and $h(F)$ it is possible to determine the influence of F on LIG resistivity ρ. To do this, you can use the expression $\rho = R_s \cdot h$, which follows from equation (2). The found dependence $\rho(h)$ is shown in Figure 7, *h*, which differs in the non-monotonic nature of the change ρ from h.

It is known that at the threshold value $F = F_0$, when pyrolysis of the PI film begins, there is an impressive decrease (up to 16 orders of magnitude) in the resistivity of its surface layer [7], since polyimide is a dielectric. At a slight exceedance of F over F_0 ($F \sim 31\,\mathrm{J/cm^2}$) there is further decrease ρ due to the formation of a continuous layer of LIG, as evidenced by the initial section of the dependence $\rho(F)$ shown in Figure 7, *h*. It also follows from this Figure that at $F \geq 67\,\mathrm{J/cm^2}$ the increase in F leads to the noticeable increase in ρ. This increase in resistivity with F increasing can be explained by structural changes in LIG that occur at large F, which is clearly demonstrated by SEM images (see Figure 4). Thus, from Figure 7, *h* it follows that ρtakes values from 0.09 to $0.13\,\Omega \cdot \mathrm{cm}$, and there is a range $F = 67 \div 110\,\mathrm{J/cm^2}$, at which LIG resistivity has minimum value. It is noteworthy that, in accordance with Raman data presented in Figure 5, *b*, in this range a minimum number of defects in LIG is observed. The values we found ρ for LIG will allow us to calculate its electrical conductivity σ. From Figure 7, *h* it follows that depending on F the electrical conductivity σ of the synthesized LIG varies in the range $7.7 \div 10\,\mathrm{S/cm}$, which is in agreement with the data of [11].

Note that the measured thickness h and conductivity ρ of LIG film structure are close to the values obtained in resistive Ag/Pd films [46], where PDE is observed [47,48], leading to the generation of a photocurrent wave vector depending on the direction [49]. PDE is also observed in LIG film structures [4,45]. However, the PDE photocurrent pulses in LIG, in contrast to the photocurrent in resistive Ag/Pd films, practically repeat the temporal shape of nanosecond laser pulses [4,45], which makes it possible to use LIG as a high-speed photodetector operating in a wide spectral range. In contrast to resistive Ag/Pd films, as well as nanographite films [50] and films from carbon nanowalls [51], synthesized by chemical vapor deposition, where the generation of orientation-sensitive „fast“ photocurrent is also observed, LIG is a cheaper material. This allows us to consider LIG film structures as inexpensive material for creating high-speed photodetectors.

4. Conclusion

Thus, in this paper, we investigate the effect of laser radiation fluence on the electrical resistance of LIG film structures formed on the surface of PI film during laser pyrolysis of its near-surface layer. Measurements of LIG sheet resistance, as well as the contact resistance and specific contact resistance between LIG and the copper electrode were carried out using the two-electrode method by determining the dependence of the resistance between the two electrodes on the distance between them. It was established that the above-mentioned electrical characteristics of LIG significantly depend on the laser fluence. In particular, the specific contact resistance between the copper electrode and LIG film structure synthesized by scanning a laser beam at speed of 220 mm/s, with increase in fluence from 31 to $137\,\mathrm{J/cm^2}$ decreased from 43 to $9\,\Omega \cdot \mathrm{mm^2}$. Measurements carried out by the four-probe technique of sheet resistance along and perpendicular to the scanning directions of the laser beam established that LIG film structure has an anisotropy of sheet resistance, which increases with fluence increasing during LIG synthesis. By determining the dependences of LIG sheet resistance and its thickness on the fluence, it was established that there is optimal fluence at which LIG resistivity has minimum value corresponding to the electrical conductivity 10 S/cm.

The results obtained can be used in the development of various sensors, the operating principle of which is based on measuring LIG resistance, which changes under external influence. The new knowledge obtained in this paper regarding the electrical properties of LIG can also be used to optimize the parameters of high-speed light-to-photocurrent converters based on LIG.

Acknowledgments

The authors are grateful to A.I. Chukavin (UdmFRC Ural Branch RAS) for analyzing the LIG samples on SEM.

Funding

The study was supported by a grant from the Russian Science Foundation No. 22-72-00017, https://rscf.ru/project/22-72-00017/. The experiments have been carried out using the equipment provided by the Shared Use Center „Center of Physical and Physicochemical Methods of Analysis and Study of the Properties and Surface Characteristics of Nanostructures, Materials, and Products“ of the Udmurt Federal Research Center, Ural Branch of RAS.

Conflict of interest

The authors declare that they have no conflict of interest.

References

[1] J. Lin, Z. Peng, Y. Liu, F. Ruiz-Zepeda, R. Ye, E.L.G. Samuel, M.J. Yacaman, B.I. Yakobson, J.M. Tour. Nature Commun. **5**, 5714 (2014).
[2] R. Ye, D.K. James, J.M. Tour. Adv. Mater. **31**, 1803621 (2019).
[3] K. Muzyka, G. Xu. Electroanalysis **34**, 574 (2022).
[4] K.G. Mikheev, R.G. Zonov, D.L. Bulatov, A.E. Fateev, G.M. Mikheev. Tech. Phys. Lett. **46**, 458 (2020).
[5] K.G. Mikheev, R.G. Zonov, T.N. Mogileva, A.E. Fateev, G.M. Mikheev. Opt. Laser Technol. **141**, 107143 (2021).
[6] A. Velasco, Y.K. Ryu, A. Hamada, A. de Andrés, F. Calle, J. Martinez. Nanomaterials **13**, 788 (2023).
[7] T. Feurer, R. Sauerbrey, M.C. Smayling, B.J. Story. Appl. Phys. A **56**, 275 (1993).
[8] B. Kulyk, B.F.R. Silva, A.F. Carvalho, P. Barbosa, A.V. Girão, J. Deuermeier, A.J.S. Fernandes, F.M.L. Figueiredo, E. Fortunato, F.M. Costa. Adv. Mater. Technol. **8**, 2101311 (2022).
[9] C.T. Long, J.H. Oh, A.D. Martinez, C.I. Sanchez, A.Sarmah, K. Arole, M.T. Rubio, M.J. Green. Carbon **200**, 264 (2022).
[10] S. Remesh, M. Vasudevan, V. Perumal, M. Ovinis, S. Karuppanan, T.N.J.I. Edison, P.B. Raja, M.N.M. Ibrahim, C.H. Voon, N. Arumugam, R.S. Kumar. J. Environ. Chem. Eng. **11**, 110600 (2023).
[11] A. Kaidarova, J. Kosel. IEEE Sens. J. **21**, 12426 (2021).
[12] P. Xue, Z. Huang, C. Chen. Lubricants **10**, 239 (2022).
[13] L. Cheng, W. Guo, X. Cao, Y. Dou, L. Huang, Y. Song, J. Su, Z. Zeng, R.Ye. Mater. Chem. Front. **5**, 4874 (2021).
[14] H. Wang, Z. Zhao, P. Liu, X. Guo. Biosensors **12**, 55 (2022).
[15] H. Zhang, Y. Zhang, C. Chen, P. Yu, L.-M. Wang, G. Li. ACS Appl. Mater. Interfaces **15**, 19170 (2023).
[16] Q. Zhang, F. Zhang, X. Liu, Z. Yue, X. Chen, Z. Wan. Adv. Mater. Technol. **8**, 2300244 (2023).
[17] S.G. Jo, R. Ramkumar, J.W. Lee. ChemSusChem. **17**, e202301146 (2023).
[18] S. Xi, X.-W. Gao, X.-M. Cheng, H.-L. Liu. New Carbon Mater. **38**, 913 (2023).
[19] A.V. Syugaev, R.G. Zonov, K.G. Mikheev, A.N. Maratkanova, G.M. Mikheev. J. Phys. Chem. Solids **181**, 111533 (2023).
[20] Y.P. Suhorukov, A.V. Telegin, K.G. Mikheev, R.G. Zonov, L.I. Naumova, G.M. Mikheev. Opt. Mater. **133**, 112957 (2022).
[21] Y. Wang, C. Han, Y. Zhou, C. Ke, Y. Fan, Y. Yang, Z. Chen, Y.S. Wang. Carbon Trends **11**, 100255 (2023).
[22] J. Liu, H. Ji, X. Lv, C. Zeng, H. Li, F. Li, B. Qu, F. Cui, Q. Zhou. Microchim. Acta **189**, 1 (2022).
[23] S.Y. Jeong, J.U. Lee, S.M. Hong, C.W. Lee, S.H. Hwang, S.C. Cho, B.S. Shin. Nanomaterials **11**, 951 (2021).
[24] Z. Wan, N.T. Nguyen, Y. Gao, Q. Li, Sustain. Mater. Technol. **25**, e00205 (2020).
[25] L. Cheng, G. Fang, L. Wei, W. Gao, X. Wang, Z. Lv, W. Xu, C. Ding, H. Wu, W. Zhang, A. Liu. ACS Appl. Nano Mater. **6**, 7290 (2023).
[26] R. Rahimi, M. Ochoa, W. Yu, B. Ziaie. ACS Appl. Mater. Interfaces **7**, 4463 (2015).
[27] Y. Zou, M. Zhong, S. Li, Z. Qing, X. Xing, G. Gong, R. Yan, W. Qin, J. Shen, H. Zhang, Y. Jiang, Z. Wang, C. Zhou. Polymers **15**, 3553 (2023).
[28] F.J. Romero, A. Salinas-Castillo, A. Rivadeneyra, A. Albrecht, A. Godoy, D.P. Morales, N. Rodriguez. Nanomaterials **8**, 517 (2018).
[29] D.K. Schroder, D.L. Meier. IEEE Trans. Electron Devices **31**, 637 (1984).
[30] K.G. Mikheev, R.G. Zonov, A.V. Syugaev, D.L. Bulatov, G.M. Mikheev. PSS **64**, 579 (2022).
[31] K.G. Mikheev, A.V. Syugaev, R.G. Zonov, D.L. Bulatov, G.M. Mikheev. PSS **65**, 347 (2023).
[32] K.G. Mikheev, T.N. Mogileva, A.E. Fateev, N.A. Nunn, O.A. Shenderova, G.M. Mikheev. Appl. Sci. **10**, 3329 (2020).
[33] G.K. Reeves, H.B. Harrison. IEEE Electron Device Lett. **EDL-3**, 111 (1982).
[34] L.X. Duy, Z. Peng, Y. Li, J. Zhang, Y. Ji, J.M. Tour. Carbon **126**, 472 (2018).
[35] M. Liu, J.N. Wu, H.Y. Cheng. Sci. China Technol. Sci. **65**, 41 (2022).
[36] L.M. Malard, M.A. Pimenta, G. Dresselhaus, M.S. Dresselhaus. Phys. Rep. **473**, 51 (2009).
[37] I.R. Hristovski, L.A. Herman, M.E. Mitchell, N.I. Lesack, J. Reich, J.F. Holzman. Nanomaterials **12**, 1241 (2022).
[38] B. Kulyk, B.F.R. Silva, A.F. Carvalho, S. Silvestre, A.J.S. Fernandes, R. Martins, E. Fortunato, F.M. Costa. ACS Appl. Mater. Interfaces **13**, 10210 (2021).
[39] J.L. Beckham, J.T. Li, M.G. Stanford, W. Chen, E.A. McHugh, P.A. Advincula, K.M. Wyss, Y. Chyan, W.L. Boldman, P.D. Rack, J.M. Tour. ACS Nano **15**, 8976 (2021).
[40] A. Minhas-Khan, S. Nambi, G. Grau. Carbon **181**, 310 (2021).
[41] J.D. Kim, T. Kim, J. Pak. Trans. Korean Inst. Electr. Eng. **67**, 406 (2018).
[42] J. de la Roche, I. López-Cifuentes, A. Jaramillo-Botero. Carbon Lett. **33**, 587 (2023).
[43] H. Tetik, E. Markgraf, K. Kato, V.N. Chan, M.H. Malakooti. Flex. Print. Electron. **8**, 035001 (2023).
[44] Y.H. Yen, C.S. Hsu, Z.Y. Lei, H.J. Wang, C.Y. Su, C.L. Dai, Y.C. Tsai. Micromachines **13**, 1220 (2022).
[45] K.G. Mikheev, A.E. Fateev, R.G. Zonov, D.L. Bulatov, G.M. Mikheev. J. Phys. Conf. Ser. **1695**, 012113 (2020).
[46] G.M. Mikheev, A.S. Saushin, O.Yu. Goncharov, G.A. Dorofeev, F.Z. Gilmutdinov, R.G. Zonov. PSS **56**, 2286 (2014).
[47] G.M. Mikheev, A.S. Saushin, V.V. Vanyukov, K.G. Mikheev, Yu.P. Svirko. PSS **58**, 2345 (2016).
[48] G.M. Mikheev, A.S. Saushin, V.V. Vanyukov, K.G. Mikheev, Y.P. Svirko. Nanoscale Res. Lett. **12**, 39 (2017).
[49] E.L. Ivchenko. Optical Spectroscopy of Semiconductor Nanostructures. Springer (2004).
[50] G.M. Mikheev, R.G. Zonov, A.N. Obraztsov, Yu.P. Svirko, A.P. Volkov. Instr. and Exp. Techn. **48**, 349 (2005).
[51] R. Zonov, A. Fateev, A. Obraztsov, G. Mikheev. Phys. Status Solidi B **260**, 2200540 (2023).

Translated by I.Mazurov